AN NBSS ALGORITHM FOR PHARMACOKINETIC ANALYSIS OF PROSTATE CANCER USING DCE-MR IMAGES

ArulMurugan Ambikapathi[†]*, Tsung-Han Chan*[†]*, Kannan Keizer*[†]*, Fei-Shih Yang*[‡]*, and Chong-Yung Chi*[†]

[†]Institute of Communications Engineering, National Tsing Hua University, Hsinchu, Taiwan
[‡]Department of Radiology, Mackay Memorial Hospital, Taipei, Taiwan
E-mail: {aareul,thchan}@ieee.org;mmh80@ms2.mmh.org.tw;cychi@ee.nthu.edu.tw;

ABSTRACT

Dynamic contrast enhanced magnetic resonance (DCE-MR) imaging is an exciting tool to study the pharmacokinetics of a suspected tumor tissue. Nonetheless, the inevitable partial volume effect in DCE-MR images may seriously hinder the quantitative analysis of the kinetic parameters. In this work, based on the conventional three-tissue compartment model, we propose an unsupervised non-negative blind source separation (nBSS) algorithm, called time activity curve (TAC) estimation by projection (TACE-Pro), to dissect and characterize the composite signatures in DCE-MR images of patients with prostate cancers. The TACE-Pro algorithm first identifies the TACs (up to a scaling ambiguity) with theoretical support. Then the problem of scaling ambiguity and the estimation of kinetic parameters is handled by pharmacokinetic model fitting. Some Monte Carlo simulations and real DCE-MR image experiments of a patient with prostate cancer were performed to demonstrate the superior efficacy of the proposed TACE-Pro algorithm. Furthermore, the real data experiments revealed the consistency of the extracted information with the biopsy results.

1. INTRODUCTION

Prostate cancer is a most common cancer in men and the number of patients with prostate cancer is considerably increasing worldwide. It is also one of the most high-risk types of cancers and it is among the leading causes of cancer deaths [1, 2]. DCE-MR imaging is a powerful imaging modality suitable for early stage diagnosis of prostate cancer. The analysis of the pharmacokinetic model of the DCE-MR images is to estimate kinetic, physiological parameters of tissues. Although the kinetic parameters have shown to be relevant to cancer diagnosis, response of therapy and the survival rate, the inevitable partial volume effect in DCE-MR images still hinders the quantitative analysis of the kinetic parameters. Partial volume effect is a phenomenon that the signal at each pixel of DCE-MR image data set is a weighted composition of time activities of more than one distinct tissue irrespective of the spatial resolution. Current methods for pharmacokinetic analysis are based on the approaches reported in [3, 4]. Major limitations of these methods include unrealistic assumption on the compartment model that the tissue kinetics are statistically independent, intractable computational complexity, and sensitivity to initialization.

In this work, for the pharmacokinetic analysis of DCE-MR images of prostate cancer, we develop an unsupervised non-negative blind source separation (nBSS) algorithm, namely time activity curve (TAC) estimation by projection (TACE-Pro), motivated by our previous work in hyperspectral image analysis (for spectral signature identification of disparate minerals in remote sensing) [5]. The TACE-Pro algorithm first identifies the TACs up to a scaling ambiguity. The issue of scaling ambiguity is then handled by pharmacokinetic model fitting, which is implemented using sequential quadratic programming (SQP) solvers. Finally, the estimation of the kinetic parameters using the obtained TACs can be formulated as a convex constrained least-squares problem and can be solved by available convex optimization solvers. The simulation and experimental results are presented to demonstrate the superior efficacy of TACE-Pro algorithm.

This work was supported in part by National Science Council (R.O.C.) under Grant NSC 99-2221-E-007-003-MY3 and in part by NTHU and Mackay memorial hospital under Grant 100N2742E1.

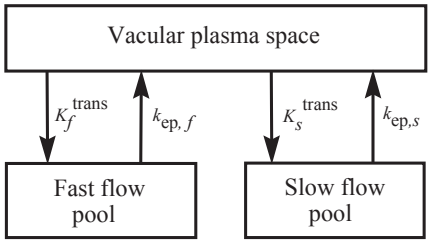

Fig. 1. Schematic diagram of three-tissue compartmental model.

The notations used in this paper are briefed as follows: $\mathbb{R}^M$ represents the set of real $M \times 1$ vectors, $\mathbf{1}_N$ represents the $N \times 1$ all-one vector, and $\mathbf{I}_N$ is the $N \times N$ identity matrix. $\otimes$ represents convolution operation. The symbol $\|\cdot\|$ represents the Euclidean norm and $\mathbf{X}^\dagger$ stands for Moore-Penrose pseudo-inverse of matrix $\mathbf{X}$.

2. PROBLEM STATEMENT

In 1991, Tofts et al. [6] proposed a compartmental model to analyze T1-weighted DCE-MR images. In the presence of tumor, the tissue compartment model consists of fast flow and slow flow pools [7], as shown in Figure 1. There are three principal parameters of interest, namely the unidirectional transfer constant (K^{trans}), the flux rate constant (k_{ep}), and the extravascular extracellular space (EES) plasma fractional volume (K_p). The dynamic tracer concentrations are governed by a set of first-order differential equations [6]:

$$\frac{dC_f(t)}{dt} + k_{\text{ep},f} C_f(t) = K_f^{\text{trans}} C_p(t), \quad (1)$$

$$\frac{dC_s(t)}{dt} + k_{\text{ep},s} C_s(t) = K_s^{\text{trans}} C_p(t), \quad (2)$$

$$C_{\text{ms}}(t) = K_p C_p(t) + C_f(t) + C_s(t), \quad (3)$$

where $C_f(t)$ and $C_s(t)$ are the tracer concentrations of the interstitial space in the fast and slow flow pools at time t, respectively; $C_p(t)$ is the tracer concentration in arterial (plasma) input function at time t; $C_{\text{ms}}(t)$ is the measured tracer concentration at time t; K_f^{trans} and K_s^{trans} (in min^{-1}) are the unidirectional transfer constants from plasma to fast and slow flow pools, respectively; $k_{\text{ep},f}$ and $k_{\text{ep},s}$ (in min^{-1}) are the flux rate constants from fast and slow flow pools to plasma, respectively. Equations (1)-(3) can be solved for $C_f(t)$ and $C_s(t)$ in terms of the rate constants and the solutions are given by

$$C_f(t) = K_f^{\text{trans}} C_p(t) \otimes \exp(-k_{\text{ep},f}\, t), \tag{4}$$

$$C_s(t) = K_s^{\text{trans}} C_p(t) \otimes \exp(-k_{\text{ep},s}\, t). \tag{5}$$

Let $a_p(t) = C_p(t), a_f(t) = C_p(t) \otimes \exp(-k_{\text{ep},f}\, t)$, and $a_s(t) = C_p(t) \otimes \exp(-k_{\text{ep},s}\, t)$. Consider the discretized signal model with temporal resolution Δt, and denote the tracer concentration measured at time $t_m = (m-1)\Delta t$ in the pixel n by $C_{\text{ms}}(n, t_m)$. Then, by (4) and (5), temporal patterns of $C_{\text{ms}}(n, t_m)$ (given by (3) in the nth pixel) can be expressed as the following latent variable model [7]:

$$\mathbf{x}[n] = [\ \mathbf{a}_p\ \ \mathbf{a}_f\ \ \mathbf{a}_s\ ]\, \mathbf{k}[n] \in \mathbb{R}^M,\ n = 1, ..., L, \tag{6}$$

where $\mathbf{x}[n] = [C_{\text{ms}}(n, t_1), \ldots, C_{\text{ms}}(n, t_M)]^T$, $\mathbf{a}_p \in \mathbb{R}^M$ is the arterial input function (AIF) which is the plasma TAC, and $\mathbf{a}_f \in \mathbb{R}^M$ and $\mathbf{a}_s \in \mathbb{R}^M$ are the TACs of fast and slow flow tissues, respectively, (which are also represented by $\mathbf{a}_j = [a_j(t_1), \ldots, a_j(t_M)]^T \in \mathbb{R}^M, j \in \{p, f, s\}$ below, for ease of the ensuing development), and $\mathbf{k}[n] = [K_p[n], K_f^{\text{trans}}[n], K_s^{\text{trans}}[n]]^T \in \mathbb{R}^3$ is a vector containing the kinetic parameters in the nth pixel. In addition, M is the number of sampling time points and L is the total number of pixels. Therefore we have

$$\mathbf{a}_f = \mathbf{D}(k_{\text{ep},f})\mathbf{a}_p, \tag{7}$$

$$\mathbf{a}_s = \mathbf{D}(k_{\text{ep},s})\mathbf{a}_p, \tag{8}$$

where $\mathbf{D}(x)$ is an $M \times M$ lower triangular matrix with the (i, j)th entry being

$$D_{ij}(x) = \begin{cases} \Delta t \exp(-(i-j)x\Delta t), & i \geq j, \\ 0, & i < j. \end{cases} \tag{9}$$

The aim of this work is to estimate TACs $\mathbf{a}_p$, $\mathbf{a}_f$, $\mathbf{a}_s$ and the kinetic parameters $\mathbf{k}[1], ..., \mathbf{k}[L]$ from the given DCE-MR data $\mathbf{x}[1], ..., \mathbf{x}[L]$. Some general assumptions are as follows:

(A1) The components of $\mathbf{k}[n]$ are non-negative.

(A2) The TACs $\mathbf{a}_p$, $\mathbf{a}_f$, $\mathbf{a}_s$ are linearly independent.

(A3) (Pure pixel assumption)
- In the entire image, there exists a pure artery pixel index l_p such that $K_f^{\text{trans}}[l_p] = K_s^{\text{trans}}[l_p] = 0$ and $K_p[l_p] \neq 0$, leading to $\mathbf{x}[l_p] = K_p[l_p]\mathbf{a}_p$.
- In the prostate gland, there exists an index set $\{l_f, l_s\}$ such that $\mathbf{x}[l_j] = K_j^{\text{trans}}[l_j]\mathbf{a}_j$ for $j \in \{f, s\}$.

(A4) (Physical assumptions) [6]
- Blood plasma volume $K_p[n] \leq 1,\ \forall n$.
- Flux rate constant is greater than transfer constant in both fast and slow flow pools, i.e., $k_{\text{ep},f} \geq K_f^{\text{trans}}[n]$ and $k_{\text{ep},s} \geq K_s^{\text{trans}}[n],\ \forall n$.
- The unidirectional transfer constant is larger in fast flow tissue than in slow flow tissue, i.e., $K_f^{\text{trans}}[n] \geq K_s^{\text{trans}}[n],\ \forall n$.

Assumptions (A1), (A2), (A4) are the assumptions widely used in DCE-MR image analysis [7]. Assumption (A3) means that within the prostate gland the distributions of the fast and slow flow tissues are not fully overlapped. Moreover, because a pure artery pixel in the prostate gland may not be acquired/imaged, we instead assume that in the entire image there exists a pure artery pixel, possibly corresponding to internal pudendal artery or inferior vesical artery or middle rectal artery.

3. TAC ESTIMATION BY PROJECTION

In this section, we propose an unsupervised nBSS algorithm, namely TAC Estimation By Projection (TACE-Pro) for pharmacokinetic analysis of DCE-MR image data.

3.1. Estimation of Pure Pixel Indices

We first present how to sequentially estimate the pure pixel indices corresponding to the TACs of plasma, fast flow, and slow flow regions, from the DCE-MR image data. The estimated pure pixel indices are then used to estimate the associated TACs and kinetic parameters, as presented in the subsequent subsection.

To begin with, we first normalize the DCE-MR data (6) as

$$\bar{\mathbf{x}}[n] \triangleq \mathbf{x}[n]/(\mathbf{1}_M^T \mathbf{x}[n]) \tag{10}$$

$$= \bar{k}_p[n]\bar{\mathbf{a}}_p + \bar{k}_f[n]\bar{\mathbf{a}}_f + \bar{k}_s[n]\bar{\mathbf{a}}_s,\ n = 1, ..., L, \tag{11}$$

where $\bar{\mathbf{a}}_j = \mathbf{a}_j/\mathbf{1}_M^T\mathbf{a}_j$ for $j \in \{p, f, s\}$ denote the normalized TACs, and $\bar{k}_p[n] = K_p[n](\mathbf{1}_M^T\mathbf{a}_p)/\mathbf{1}_M^T\mathbf{x}[n]$ and $\bar{k}_j[n] = K_j^{\text{trans}}[n](\mathbf{1}_M^T\mathbf{a}_j)/\mathbf{1}_M^T\mathbf{x}[n]$ for $j \in \{f, s\}$ are the normalized kinetic parameters. It can be easily verified that

$$\sum_{i \in \{p,f,s\}} \bar{k}_i[n] = 1. \tag{12}$$

With the normalized data (10), the first pure pixel index, l_p, can be estimated. It has been proved in [8] that by (12) and under (A1)-(A3) the normalized AIF and its pure pixel index can be identified by

$$\boxed{\bar{\mathbf{a}}_p = \bar{\mathbf{x}}[l_p],\ l_p \in \arg\max_{n \in \mathcal{I}} \{\|\bar{\mathbf{x}}[n]\|\},} \tag{13}$$

where $\mathcal{I}$ is the set of pixel indices over the entire image.

Next, the question that remains is how to estimate the rest of the pure pixel indices, say $\{l_f, l_s\}$. Though in this work we have considered the three-tissue compartment model with total number of tissue compartments $N = 3$, in the ensuing development, the normalized model in (10) can be generalized to any N tissue compartments as

$$\bar{\mathbf{x}}[n] = \sum_{j=1}^{N} \bar{k}_j[n]\bar{\mathbf{a}}_j,\ n = 1, ..., L, \tag{14}$$

where $\bar{k}_1[n] = \bar{k}_p[n]$, and $\bar{\mathbf{a}}_1 = \bar{\mathbf{a}}_p$ has been estimated by (13). To estimate the pure pixel indices $\{l_j\}_{j=2}^N$ in a sequential manner, we first obtain the mean-removed data

$$\tilde{\mathbf{x}}[n] = \bar{\mathbf{x}}[n] - \bar{\boldsymbol{\mu}} = \sum_{i=1}^{N} \bar{k}_i[n]\boldsymbol{\beta}_i, \tag{15}$$

where $\bar{\boldsymbol{\mu}} = \sum_{n=1}^{L} \bar{\mathbf{x}}[n]/L$ is the mean of the normalized data, and $\boldsymbol{\beta}_i = \bar{\mathbf{a}}_i - \bar{\boldsymbol{\mu}}$ is the unknown mean-removed TACs. Suppose that the mean-removed TACs $\boldsymbol{\beta}_1, ..., \boldsymbol{\beta}_j$ (where $j < N$) have already been identified. To identify the next mean-removed TAC $\boldsymbol{\beta}_{j+1}$, we first find a normal vector [9] to the affine set formed by $\boldsymbol{\beta}_1, ..., \boldsymbol{\beta}_j$:

$$\mathbf{d}^\star = \arg \min_{\mathbf{d} \in \text{aff}\{\boldsymbol{\beta}_1, \ldots, \boldsymbol{\beta}_j\}} \|\mathbf{d}\|^2 = \mathbf{P}_{\mathbf{B}}^{\perp}\boldsymbol{\beta}_j, \tag{16}$$

where aff$\{\boldsymbol{\beta}_1,\ldots,\boldsymbol{\beta}_j\} = \{\boldsymbol{y} = \sum_{i=1}^{j}\vartheta_i\boldsymbol{\beta}_i | \mathbf{1}_j^T\boldsymbol{\vartheta} = 1, \boldsymbol{\vartheta}\in\mathbb{R}^j\}$ in which $\boldsymbol{\vartheta} = [\vartheta_1,\ldots,\vartheta_j]^T$ [9], and $\mathbf{P}_{\mathbf{B}}^{\perp} = \mathbf{I}_{N-1} - \mathbf{B}\mathbf{B}^{\dagger}$ is the orthogonal complement projector of $\mathbf{B} \triangleq [\boldsymbol{\beta}_1 - \boldsymbol{\beta}_j,\ldots,\boldsymbol{\beta}_{j-1} - \boldsymbol{\beta}_j] \in \mathbb{R}^{(N-1)\times(j-1)}$. Then, by (A1), (A3), and (15), we have

$$\tilde{\mathbf{x}}[n]^T\mathbf{d}^{\star} = \sum_{i=1}^{N}\bar{k}_i[n]\boldsymbol{\beta}_i^T\mathbf{d}^{\star} \geq \min_{i=1,\ldots,N}\{\boldsymbol{\beta}_i^T\mathbf{d}^{\star}\}. \quad (17)$$

where the equality holds if and only if $n = l_z$ (a pure pixel index) for any $z \in \arg\min_i\{\boldsymbol{\beta}_i^T\mathbf{d}^{\star}\}$. Following the proof in [5, Lemma 2] and assuming that $\boldsymbol{\beta}_i^T\mathbf{d}^{\star},\ i = 1,\ldots,N$ are distinct, one can show that under (A1)-(A3), the new mean-removed TAC and its pure pixel index can be estimated by

$$\boxed{\tilde{\mathbf{x}}[l_z] \in \{\boldsymbol{\beta}_{j+1},...,\boldsymbol{\beta}_N\},\ l_z \in \arg\min_{n=1,\ldots,L}\tilde{\mathbf{x}}[n]^T\mathbf{d}^{\star}.} \quad (18)$$

The above procedure given by (16) and (18) will be repeated until all the rest of pure pixel indices $\{l_j\}_{j=2}^{N}$ are found.

3.2. Estimation of TACs and Kinetic Parameters

Given the pure pixel indices $\{\hat{l}_p,\hat{l}_2,\hat{l}_3\} = \{\hat{l}_p,\hat{l}_f,\hat{l}_s\}$ (for $N = 3$) estimated above, by (6)-(8) and (A3), we have

$$\hat{\mathbf{a}}_p \ = \ \mathbf{x}[\hat{l}_p]/K_p[\hat{l}_p], \quad (19)$$

$$\mathbf{x}[\hat{l}_j] \ = \ K_j^{\text{trans}}[\hat{l}_j]\,\hat{\mathbf{a}}_j \ = \ K_j^{\text{trans}}[\hat{l}_j]\,\mathbf{D}(k_{\text{ep},j})\,\hat{\mathbf{a}}_p,\ j\in\{2,3\}. \quad (20)$$

Substituting (19) into (20) yields

$$\mathbf{x}[\hat{l}_j] = K_j^{\text{trans}}[\hat{l}_j]\mathbf{D}(k_{\text{ep},j})\mathbf{x}[\hat{l}_p]/K_p[\hat{l}_p], \quad j\in\{2,3\}, \quad (21)$$

where $\mathbf{x}[\hat{l}_p]$, $\mathbf{x}[\hat{l}_2]$, and $\mathbf{x}[\hat{l}_3]$ are known. Hence, based on (A4), we can estimate the kinetic parameters for the tissue TACs by the following non-negative least-squares problem

$$\min_{\substack{0\leq K_p[\hat{l}_p]\leq 1,\\ 0\leq K_j^{\text{trans}}[\hat{l}_j]\leq k_{\text{ep},j},\\ j\in\{2,3\}}}\ \sum_{j\in\{2,3\}}\|\mathbf{x}[\hat{l}_j] - \frac{K_j^{\text{trans}}[\hat{l}_j]}{K_p[\hat{l}_p]}\mathbf{D}(k_{\text{ep},j})\mathbf{x}[\hat{l}_p]\|^2. \quad (22)$$

The above nonconvex problem can be handled by using sequential quadratic programming (SQP) [10] solvers. By (A4) (w.l.o.g), if $\hat{k}_{\text{ep},2} > \hat{k}_{\text{ep},3}$, then $\hat{k}_{\text{ep},f} = \hat{k}_{\text{ep},2}$, $\hat{k}_{\text{ep},s} = \hat{k}_{\text{ep},3}$, $\hat{K}_f^{\text{trans}}[\hat{l}_f] = \hat{K}_2^{\text{trans}}[\hat{l}_2]$, and $\hat{K}_s^{\text{trans}}[\hat{l}_s] = \hat{K}_3^{\text{trans}}[\hat{l}_3]$. Denoting a solution of (22) by $\{\hat{K}_f^{\text{trans}}[\hat{l}_f],\ \hat{k}_{\text{ep},f},\ \hat{K}_s^{\text{trans}}[\hat{l}_s],\ \hat{k}_{\text{ep},s},\ \hat{K}_p[\hat{l}_p]\}$, then the true AIF $\hat{\mathbf{a}}_p$, and the tissue TACs $\hat{\mathbf{a}}_f$, $\hat{\mathbf{a}}_s$ can be estimated by

$$\hat{\mathbf{a}}_p = \mathbf{x}[\hat{l}_p]/\hat{K}_p[\hat{l}_p], \quad \text{(by (19))} \quad (23)$$

$$\hat{\mathbf{a}}_j = \mathbf{D}(\hat{k}_{\text{ep},j})\hat{\mathbf{a}}_p,\ j\in\{f,s\}. \quad \text{(by (7) and (8))} \quad (24)$$

Finally, based on (6), we can estimate the kinetic parameters for every pixel by solving

$$\hat{\mathbf{k}}[n] \ = \ \arg\min_{\substack{0\leq K_p[n]\leq 1,\\ 0\leq K_s^{\text{trans}}[n]\leq K_f^{\text{trans}}[n]}}\|\mathbf{x}[n] - [\hat{\mathbf{a}}_p\ \hat{\mathbf{a}}_f\ \hat{\mathbf{a}}_s]\mathbf{k}[n]\|^2, \quad (25)$$

for $n = 1,...,L$. Problem (25) is convex and can be solved by standard convex optimization solvers, such as SeDuMi [11] and CVX [12].

The entire procedure described above is the proposed TACE-Pro algorithm that estimates the TACs $(\hat{\mathbf{a}}_p,\hat{\mathbf{a}}_f,\hat{\mathbf{a}}_s)$, flux rate constants $(\hat{k}_{\text{ep},f},\hat{k}_{\text{ep},s})$, and the maps of kinetic parameters $(\hat{\mathbf{k}}[n],\ \forall n)$.

.

Table 1. Mean±standard deviation of the estimated flux rate constants $(\hat{k}_{\text{ep},f},\hat{k}_{\text{ep},s})$ obtained by TACE-Pro algorithm over 100 independent runs for different random tissue maps and different SNRs.

SNR (dB)	$\hat{k}_{\text{ep}}$	**Scenario 1:** $k_{\text{ep},f} = 1.625$ $k_{\text{ep},s} = 0.33$	**Scenario 2:** $k_{\text{ep},f} = 3.25$ $k_{\text{ep},s} = 0.33$	**Scenario 3:** $k_{\text{ep},f} = 6.5$ $k_{\text{ep},s} = 0.33$
20	$\hat{k}_{\text{ep},f}$	1.96±0.06	3.80±0.14	9.07±1.18
	$\hat{k}_{\text{ep},s}$	0.40±0.01	0.40±0.01	0.41±0.01
30	$\hat{k}_{\text{ep},f}$	1.73±0.07	3.46±0.05	6.88±0.19
	$\hat{k}_{\text{ep},s}$	0.35±0.01	0.35±0.00	0.35±0.00
40	$\hat{k}_{\text{ep},f}$	1.66±0.01	3.31±0.07	6.62±0.07
	$\hat{k}_{\text{ep},s}$	0.33±0.00	0.33±0.00	0.33±0.00

4. SIMULATIONS

Since exact ground truths are not available for real DCE-MR image data, the performance of the proposed nBSS algorithm, TACE-Pro, is first evaluated with simulated data. To the best of our knowledge, the proposed TACE-Pro is the first nBSS algorithm specifically designed for DCE-MR image analysis of prostate cancer, and hence it is alone considered for the simulations. In the simulations, the number of compartment N was set to 3. The AIF $\mathbf{a}_p$ was generated by the population average model [13] with temporal resolution $\Delta t = 4$ seconds for 8-min period ($M = 120$), and the fast and slow TACs, $\mathbf{a}_f$ given by (7) and $\mathbf{a}_s$ given by (8), can also be generated by using $k_{\text{ep},f} \in \{1.625, 3.25, 6.5\}$ and $k_{\text{ep},s} = 0.33$. We then generated $L = 5000$ DCE-MR image pixels $\mathbf{x}[n]$ defined in (6) by using the following parameters: fast flow maps generated with $K_f^{\text{trans}} \in \{0.5, 1, 2\}$, slow flow maps generated with $K_s^{\text{trans}} = 0.1$, and plasma maps generated with $K_p[n] = 0.05$. **Scenario 1:** $(K_f^{\text{trans}}[n], k_{\text{ep},f}) = (0.5, 1.625)$ is to simulate the tissue of early-stage tumor; **Scenario 2:** $(K_f^{\text{trans}}[n], k_{\text{ep},f}) = (1, 3.25)$ is to stimulate tissue of moderate tumor; **Scenario 3:** $(K_f^{\text{trans}}[n], k_{\text{ep},f}) = (2, 6.5)$ is to simulate the tissue of active tumor. Moreover, the observed pixel vectors $\mathbf{x}[n]$ were artificially added with Gaussian white noise with zero mean and covariance matrix $\sigma^2\mathbf{I}_M$ so as to satisfy the signal-to-noise ratio (SNR) specification SNR $\triangleq \sum_{n=1}^{L}\|\mathbf{x}[n]\|^2/\sigma^2 ML$ where σ^2 is the noise variance. Table 1 shows the mean±standard deviation of the flux rate constants $(\hat{k}_{\text{ep},f},\hat{k}_{\text{ep},s})$ estimated by TACE-Pro algorithm over 100 independent runs for different random tissue maps and for different SNRs. In each run, while solving (22), five different sets of random initializations were used and the estimates with the least fitting error were considered as the solution for (22). It can be seen that in all the three scenarios, as the SNR increases, the mean values of the estimates get closer to the true values of the respective flux rate constants, and the standard deviations approach zero.

5. EXPERIMENTAL RESULTS

In real data experiments, we demonstrate the efficacy of the proposed method with T1-weighted DCE-MR images of a 72-year-old patient who has been confirmed to have prostate cancer based on biopsies. The DCE-MR image data set was acquired at Mackay Memorial Hospital, Taipei, Taiwan using Philips Achieva 3-Tesla MRI scanner. The acquired three-dimensional data set with 4 mm slice thickness, 0.45 mm pixel spacing, 10° field of view, and in-plane matrix size 256×256 were taken every 30 seconds for a total of 10 minutes after the injection of gadolinium DTPA. Figure 2 shows the biopsy results of the patient, where each percentage number denotes the proportion of tissue in that area containing cancer tissue. For this real data set, TACE-Pro algorithm has been applied while fixing $N = 3$. Figure

3(a) shows the estimated TACs both before (discrete points) and after (continuous curves) model fitting for slices 12, 15, 18, and 22. Figure 3(b) shows the corresponding estimated kinetic parameter maps. It can be observed that the slow flow TAC has lower washout rate $\hat{k}_{ep,s}$, and $\hat{k}_{ep,f}$ is much higher than $\hat{k}_{ep,s}$. Also, the fast flow tissue for all the slices are almost dominant in both sides of peripheral and central zones of the prostate gland, while the plasma volume and the slow flow tissue are relatively inactive. These results are highly consistent with the biopsy results (Figure 2).

6. CONCLUSION

We have presented an effective TAC estimation algorithm, namely TACE-Pro, followed by estimation of kinetic parameters through pharmacokinetic model fitting, for prostate DCE-MR image analysis. We have evaluated the TACE-Pro algorithm with the synthetic DCE-MRI data and real DCE-MRI images with prostate cancer. Simulation results have shown that the proposed method TACE-Pro performs well for all the scenarios (early-stage, moderate, and active tumor). For real data experiments, we have estimated the tissue TACs, kinetic parameter values, and kinetic parameter maps, which show high consistency with the biopsy results.

7. REFERENCES

[1] A. Jemal, R. Siegel, E. Ward, T. Murray, J. Xu, C. Smigal, and M. J. Thun, "Cancer statistics, 2010," *CA: A Cancer Journal for Clinicians*, vol. 60, no. 5, pp. 277-300, Sep. 2010.

[2] M. A. Khan and A. W. Partin, "Management of patients with an increasing prostate-specific antigen after radical prostatectomy," *Current Urology Reports*, vol. 3, no. 3, pp. 179-187, Jun. 2004.

[3] M. D. Plumbley, "Algorithms for non-negative independent component analysis," *IEEE Trans. Neural Netw.*, vol. 14, no. 3, pp. 534-543, May 2003.

[4] D. D. Lee and H. S. Seung, "Learning the parts of objects by non-negative matrix factorization," *Nature*, vol. 401, no. 6755, pp. 788-791, Aug. 1999.

[5] A. Ambikapathi, T.-H. Chan, C.-Y. Chi, and K. Keizer, "Two effective and computationally efficient pure-pixel based algorithms for hyperspectral endmember extraction," *in Proc. IEEE ICASSP-2011*, Prague, Czech Republic, May 22-27, 2011, pp. 1369-1372.

[6] P.S. Tofts and A.G. Kermode, "Measurement of the blood-brain barrier permeability and leakage space using dynamic MR imaging. 1. Fundamental concepts," *Magnetic Resonance in Medicine*, vol. 17, pp. 357-367, Feb. 1991.

[7] Y. Wang, 1. Xuan, R. Srikanchana, and P. L. Choyke, "Modeling and reconstruction of mixed functional and molecular patterns," *International Journal of Biomedical Imaging*, Article ID: 29707, pp. 1-9, 2006.

[8] Y.-C. Lin, T.-H. Chan, C.-Y. Chi, S.-H. Ng, H.-L. Liu, K.-C. Wei, Y.-Y. Wai, C.-C. Wang, and J.-J. Wang, "Blind estimation of arterial input function in dynamic contrast-enhanced MRI using purity maximization," to appear in *Magnetic Resonance in Medicine*, 2012.

[9] S. Boyd and L. Vandenberghe, *Convex Optimization*, UK: Cambridge Univ. Press, 2004.

[10] P. T. Boggs and J. W. Tolle, "Sequential quadratic programming," *Acta Numerica*, pp. 1-51, 1996.

[11] J. F. Sturm, "Using SeDuMi 1.02, a MATLAB toolbox for optimization over symmetric cones," *Optimiz. Methods Softw.*, vol. 11–12, pp. 625–653, 1999.

[12] M. Grant and S. Boyd. CVX: Matlab software for disciplined convex programming, version 1.21. http://cvxr.com/cvx, Oct. 2010.

[13] C. Yang, G. S. Karczmar, M. Medved and W. M. Stadler, "Estimating the arterial input function using two reference tissues in dynamic contrast-enhanced MRI studies: Fundamental concepts and simulations," *Magnetic Res. in Medicine*, vol. 52, pp. 1110-1117, Nov. 2004.

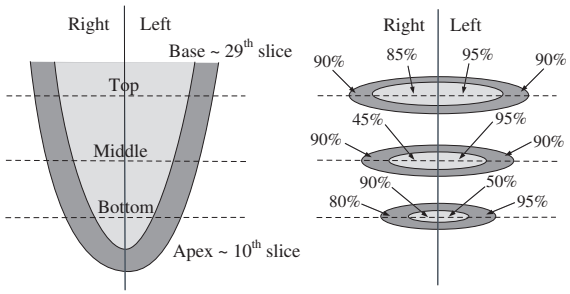

Fig. 2. Position of biopsy examination (left) and biopsy examination results showing the percentage of tumor tissues (right).

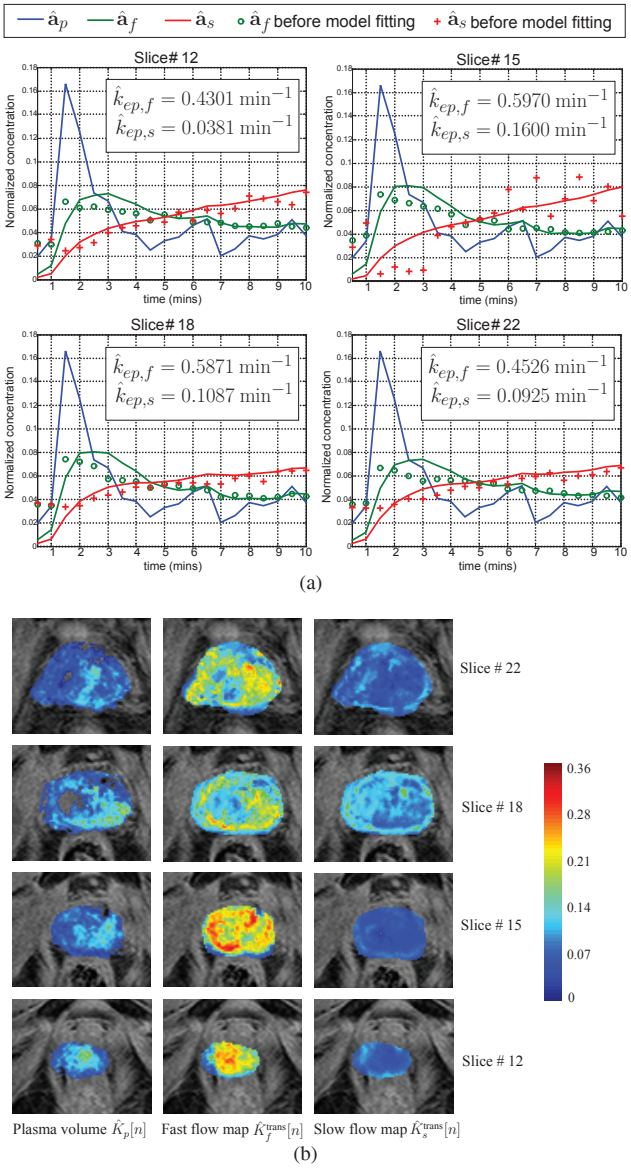

Fig. 3. (a) The estimated TACs $\hat{\mathbf{a}}_p, \hat{\mathbf{a}}_f, \hat{\mathbf{a}}_s$ (normalized such that $\mathbf{1}_M^T\hat{\mathbf{a}}_p = \mathbf{1}_M^T\hat{\mathbf{a}}_f = \mathbf{1}_M^T\hat{\mathbf{a}}_s = 1$), for slices 12, 15, 18, and 22 using TACE-Pro algorithm, and (b) the estimated kinetic parameter (or tissue) maps corresponding to the model fitted TACs in (a).